Ductile tensile failure in metals through initiation and growth of nanosized voids

Yizhe Tang [a], Eduardo M. Bringa [b], Marc A. Meyers [a,*]

[a] *University of California, San Diego, La Jolla, CA 92093, USA*
[b] *CONICET and Instituto de Ciencias Básicas, Universidad Nacional de Cuyo, Mendoza 5500, Argentina*

Abstract

We here reveal the initiation of ductile failure in metals at the nanometer scale by molecular dynamics simulations coupled with a novel analytical model. This proceeds by the emission of a special type of dislocation shear loop, which can expand as a partial or perfect dislocation, evolve into a prismatic loop through reaction, or develop into twins. Molecular dynamics (MD) simulations predict a strong dependence of the stress required for the initiation of plastic flow at the surface of the void for both Cu (a model fcc metal) and Ta (a model bcc metal). The decrease in stress with increasing void size is also analyzed in terms of a new analytical approach based on the energetics of dislocation loop emission. For both fcc (copper) and bcc (tantalum) metals initiation of plastic flow in MD simulations takes place at voids as small as a tri-vacancy (radius $R \approx 0.1$ nm). Extensive calculations for tantalum combined with the analytical model, which tracks the simulations, enable extrapolation to $R \approx 300$ nm, in the realm of second phase particles and inclusions. Thus we conclude that this is a general mechanism of tensile failure in pure monocrystalline metals where other initiation sites are absent.
© 2012 Acta Materialia Inc. Published by Elsevier Ltd. All rights reserved.

Keywords: Void growth; Dislocation; Ductile failure; Molecular dynamics

1. Introduction

There are two extremes of failure mechanisms when metals separate under tensile forces: (a) ductile failure by void initiation, growth, and coalescence; (b) brittle failure by crack initiation, propagation, growth, and bifurcation. The first involves plastic deformation while the latter is, *strictu sensu*, a bond breaking process. For engineering materials there are important intermediate regimes of crack propagation involving void initiation and growth ahead of the crack tip [1]. Dislocation emission from the crack tip is also an important toughening mechanism [2]. Strain rate, temperature, and stress state are three external parameters that can have a profound effect on the mechanisms. Body centered cubic (bcc) metals are particularly affected by these parameters, and can exhibit both brittle and ductile

fracture. The technological implications of this transition are of primary importance. Weertman [3] proposed a criterion for the ductile to brittle transition. The Weertman criterion [3] uses the ratio between tensile and shear strength; if $\sigma_{Shear}/\sigma_{Tensile} > 7$ the material fails in a brittle manner. However, face centered cubic (fcc) metals can also exhibit diverse failure mechanisms, with high strain rate tensile loading (such as spalling) favoring intergranular fracture over transgranular fracture, which occurs at low strain rates. Indeed, this was observed for copper [4–6].

Ductile failure is initiated in regions that cannot support the local stresses and proceeds by plastic deformation as voids grow. In engineering alloys these regions are ubiquitous: inclusions, second phase particles, grain boundaries, local regions with high stresses, and vacancy complexes. The potency of these sites, i.e. the stress at which they are activated, varies widely in metals. It is well known that in high purity metals the ductility is quite high and that they often exhibit a knife-edge fracture. Conversely, the

* Corresponding author. Tel.: +1 858 534 4719 / 858 534 5698
 E-mail address: mameyers@ucsd.edu (M.A. Meyers).

presence of second phases and inclusions has a deleterious effect on ductility [7].

Molecular dynamics is a powerful tool to interrogate representative volumes of metals of up to 10^7 nm^3 at times on the order of 10^{-9} s. It is well suited to investigate dislocation effects. Exhaustive molecular dynamics (MD) simulations of deformation in fcc metals have been carried out, focusing on dislocation configurations [8–10], plastic deformation [11], grain size effects [12–14], and void initiation and growth [15–19]. However, bcc metals have not been the subject of the same number of studies. One of the main reasons is the difficulty of implementing adequate interatomic potential functions which work properly at the large stresses and strains reached during void deformation.

We here report the results of a systematic investigation of the effect of void size on the stress required for the initiation of plastic flow. We have established the minimum void for which initiation of plastic flow takes place. The computational predictions are coupled with a new physically based analytical model which enables extension of this mechanism to void radii of 300 nm. This is in the realm of second phase particles and this mechanism thus has a multiscale character.

One may argue that the simple emission of a shear loop from a void cannot lead to its increase in size, and this is

indeed correct [20] if the loops detach from the void. This is why the emission of prismatic loops is easier to conceptualize as a mechanism for void growth. Indeed, both types of loops were considered in an earlier analytical model [21]. Shear loops in void expansion are special and their extremities remain attached to the void surface. We here present an argument developed earlier [22] for the formation and growth of a void by coordinated shear in two or more planes. The simple two-dimensional analog scheme presented in Fig. 1a illustrates this. Let us imagine a body of rectangular section composed of four trapezoidal blocks and let us assume that the four inclined interfaces are cohesive (i.e. they can slide but cannot separate) and that the vertical interface is free. When traction is applied horizontally, as shown in Fig. 1b, the two trapezoidal blocks move vertically through shear along the four glissile interfaces. In doing so they produce a lateral extrusion of material and create an internal void. Volume constancy is obeyed. Fig. 1c shows the same case for numerous glissile interfaces along two non-parallel shear planes. Coordinated shear along these interfaces produces the same transfer of material. These unit glide processes, which are in this case confined in the material, can be considered as dislocations. Each one creates a step on the void surface. In the general three-dimensional case several (five or more) slip systems
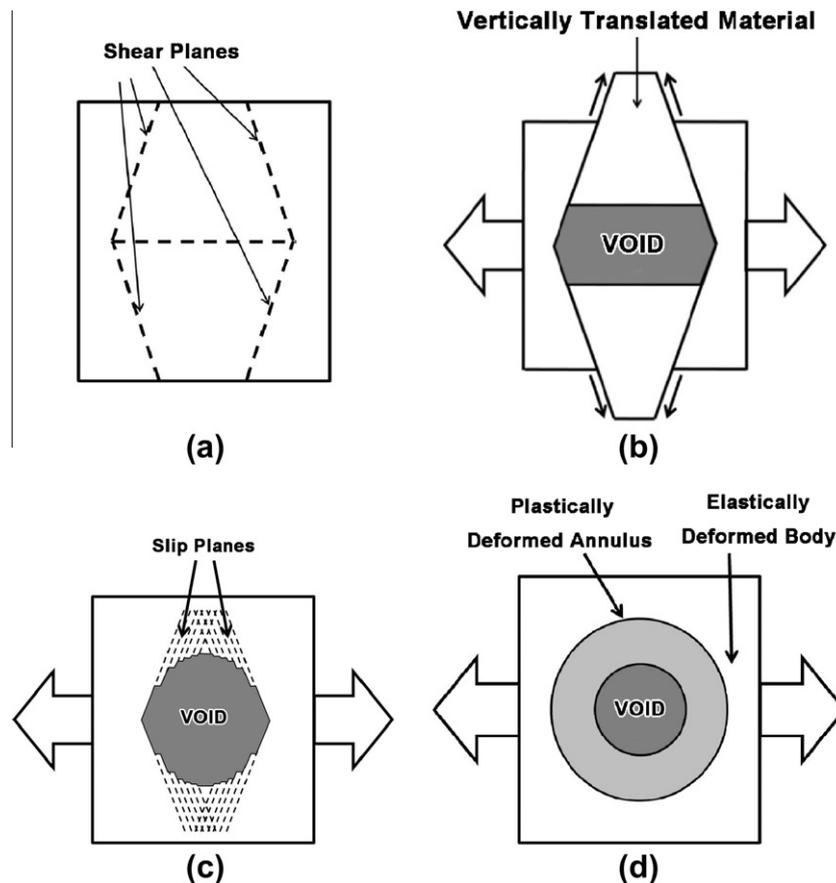

Fig. 1. (a) Initial configuration of the material decomposed into cohesive sliding trapezoidal blocks. (b) Coordinated shear of blocks generating voids and translating material outwards. (c) Coordinated shear by dislocation terminating in the body of the material. (d) Schematic representation of void growth with an annulus of plastic deformation and an elastically deformed area (adapted from Bringa et al. [22]).
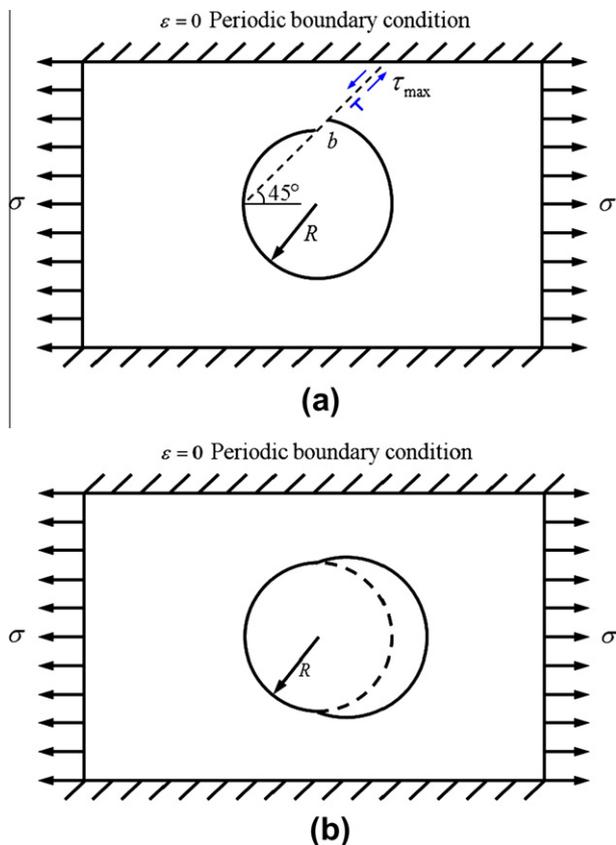
Fig. 2. Schematic showing the uniaxial tensile strain loading of a sample with a void and emission of a dislocation from the plane of maximum shear: (a) side view; (b) top view.

can be activated simultaneously or sequentially, creating the necessary material transfer operation. This region with dislocations forms a plastic annulus (which has a radius that is a multiple of the void radius). This plastic annulus is surrounded by the elastically deformed material, a classic plasticity problem. Fig. 1d shows the two regions.

The formation of shear loops is shown in Fig. 2. The side view shows the plane of maximum shear stress making an angle of 45° with the tangent to the sphere. One plane is shown, and the emission of a dislocation is represented. As the shear loop is emitted the region is shifted and the void radius consequently increases. Fig. 2b shows the top view, with the loop curving out.

These loops were analyzed in detail in previous works by our group [15,16,21,23,24]. Marian et al. [17,18], using the quasi-continuum (QC) method, were the first to identify shear loops in aluminum subjected to shear. Seppälä et al. [19] followed, using MD, but interpreted them as prismatic loops. Traiviratana et al. [15] and Bringa et al. [16] analyzed the shear loops and determined the detailed crystallographic nature and interactions of the partial dislocations. Seppälä et al. [19] identified the leading and trailing partial dislocations (Fig. 2 in Seppälä et al. [19]) in an fcc crystal and speculated that at a later stage (higher stress) the loops

would completely separate from the void surface. Fig. 3 in Seppälä et al. [19] is interpreted as representing a prismatic loop, but is more probably a section through a shear loop in which the leading and trailing partials represent the extremities of the segments circled. Hence the results of Traiviratana et al. [15] and Bringa et al. [22] are in full agreement with their MD simulations and confirm the mechanism postulated by Lubarda et al. [21].

2. Computational methods

We carried out MD simulations using LAMMPS [25] with the extended Finnis–Sinclair potential [26] which gives the correct elastic constants at zero pressure and reproduces the pressure dependence of the specific volume up to values close to 500 GPa. The extended Finnis–Sinclair potential was tested by verifying the gamma surface [27] and comparing it with ab initio results.

We used Ta bcc single crystals with periodic boundary conditions in all directions and studied uniaxial strain loading along [0 0 1] (z-direction) in tension. The samples were cubic, with sizes $L = 30$, 50, 60, 80, 100, 200 and 400 a_0, where $a_0 = 0.303$ nm is the lattice constant, with the number of atoms in the sample being $N_{sample} = 54,000$, 250,000, 432,000, 1,024,000, 2,000,000, 16,000,000 and 128,000,000. Simulations were carried out on a number of computer systems, from single core workstations to TeraGrid Supercomputers using 512 cores. In MD simulations the stress components were obtained using the nominal sample volume V_{sample}, not the real volume ($V_{sample} - V_{void}$). Therefore the stresses were corrected by multiplying a factor of $V_{sample}/(V_{sample} - V_{void})$ to eliminate the volume error in MD simulations when a void is present, where V_{sample} is the initial volume of the sample, and V_{void} is the initial volume of the void. For copper the simulation procedure was given in Traiviratana et al. [15].

The samples were thermalized at 300 K for 10 ps, using $a_0 = 0.303$ nm, but there is no thermostating during loading to capture possible plastic heating effects. We used NVE integration with a time step of 1–2 fs. The common neighbor analysis (CNA) [28] filter was used to reveal the defects (non-bcc atoms) generated by plastic deformation in Ta, and the centro-symmetry parameter (CSP) [29] filter was used for Cu.

3. Results and discussion

3.1. Mechanism of shear loop emission

The detailed nature of loop emission in fcc metals was described by Traiviratana et al. [15] and Bringa et al. [24] and for bcc metals by Tang et al. [23]. We here present the basic characteristics of the initiation of loop formation and their propagation. Fig. 3 shows a void under hydrostatic tensile loading in tantalum. In Fig. 3a a shear loop is starting to form at the surface, whereas in Fig. 3b the shear loops are well formed and glide along several slip
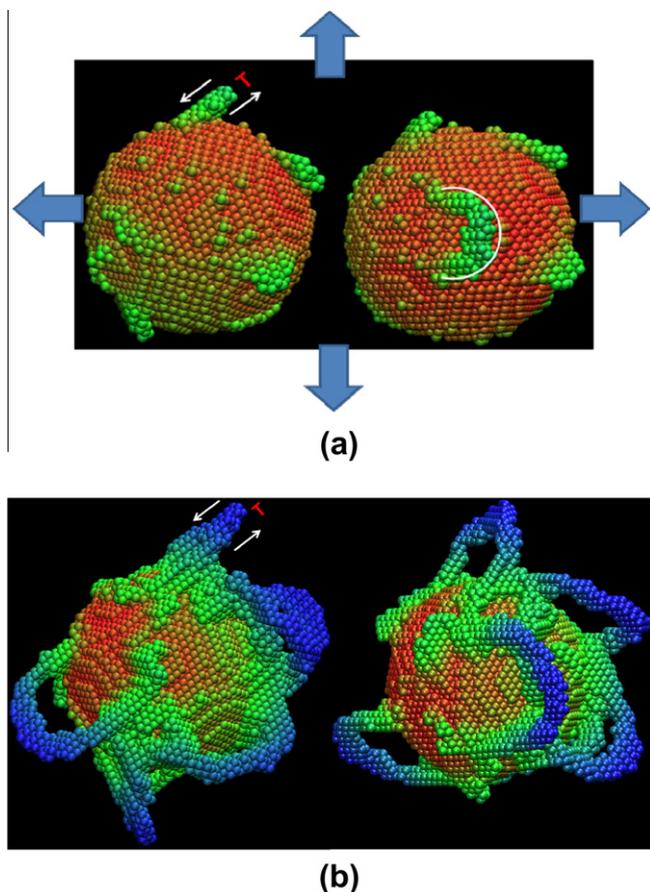
(a)

(b)

Fig. 3. Side and top views of (a) initiation of shear loop formation and (b) a more advanced stage, showing propagating loops. The direction of the resolved shear stress and the sign of dislocation are indicated on the side view. Note loops terminating on the void surface on several slip systems; hydrostatic tensile loading at a strain rate of $10^8 \, s^{-1}$, initial void radius $R = 3.3$ nm.

planes around the void surface. The shear stress direction as well as the dislocation sign are shown for one of the loops. Since the stress state is hydrostatic the loops being generated on the different slip systems have the same resolved shear stress and grow at the same velocity. The edge component of the dislocation which forms the central part of the loops has a greater mobility and advances. It should be noted that the slip plane zig-zags along two $(1\,1\,0)$ and $(0\,1\,1)$ planes. This was discussed in greater detail by Tang et al. [23]. The dislocation extremities remain embedded in the surface of the void in Fig. 3, but the dislocations may react and form prismatic loops if the loading is hydrostatic, as discussed in Tang et al. [23].

3.2. Void size effects

Fig. 2 shows the configuration used in the simulations with a void in the center. It was postulated by Lubarda et al. [21] and demonstrated through MD simulations in fcc metals that void growth and collapse take place through the emission of dislocation loops at planes making an angle of 45° with the void surface. These are the planes in which

the shear stress is maximum (radial stresses at the void surface equal to zero).

The effect of strain rate was established first. The maximum shear stresses σ_{max} (global stress averaged over the whole sample, $\sigma_{max} = (\sigma_{zz} - \sigma_{xx})/2$ or $(\sigma_{zz} - \sigma_{yy})/2)$ for defect nucleation for $R = 2$ nm at strain rates of 10^7, 10^8 and $10^9 \, s^{-1}$ are quite close under uniaxial tensile strain, despite the fact that the evolution of the stress–strain curves are different. Values of 6.22, 6.29, and 6.48 GPa, respectively, were found for $R = 2$ nm at the above strain rates. Two values of the shear modulus were used for normalization of the maximum shear stresses: shear modulus of $\{1\,1\,0\}$ planes in the $\langle 1\,1\,1 \rangle$ direction $G_{\langle 111 \rangle}$ for tantalum (bcc) and shear modulus of $\{1\,1\,1\}$ planes in the $\langle 1\,1\,2 \rangle$ direction $G_{\langle 112 \rangle}$ for copper (fcc).

For tantalum the normalized maximum shear stress $\sigma_{max} /G_{\langle 111 \rangle}$ for the initiation of plastic deformation was calculated using $G_{\langle 111 \rangle} = 52.8$ GPa and $v_{\langle 111 \rangle} = 0.275$ [30], where $v_{\langle 111 \rangle}$ is the Poisson ratio of $\{1\,1\,0\}$ planes in the $\langle 1\,1\,1 \rangle$ direction. It is plotted as a function of void radius (normalized to the Burgers vector b) in Fig. 4a. Typical errors in the plastic strain and maximum shear stress at nucleation were 1% and 2%, respectively. We normalized the maximum shear stress and void radius using the shear modulus and typical Burgers vector b ($|b| = \sqrt{3}/2 \, a_0 = 0.286$ nm) to make them amenable to comparison with other bcc metals. As can be seen in Fig. 4a, for smaller radii ($R/b \leqslant 1$–2) the stresses asymptotically approach a value of $\sigma_{max}/G_{\langle 111 \rangle} \approx 0.07$, which is the required stress for homogeneous nucleation of defects in a perfect sample ($R = 0$). This homogeneous nucleation threshold is somehow lower than the unrelaxed ideal strength of the material at 0 K [31] ($\sim 0.12 \, G_{\langle 111 \rangle}$ using the definition of $G_{\langle 111 \rangle}$ in Turley et al. [30]). As the void radius increases the maximum shear stress for tantalum $\sigma_{max} / G\langle 111\rangle$ decreases and asymptotically approaches a constant value of 0.0235 when the void size R/b exceeds ~ 100. In previous work on bcc metals using Finnis Sinclair potentials [32,33] Rudd [34] observed a decrease of 24% in the threshold stress to initiate plastic activity under hydrostatic loading for $R = 12.5$ nm (von Mises stress 12.85 GPa), compared with $R = 1.89$ nm (von Mises stress 16.49 GPa). A similar dependence of nucleation stress on void size was reported for the bcc metal vanadium [35] subject to uniaxial tensile strain.

For fcc copper the homogeneous nucleation stress reported by Bringa et al. [24] was $\sigma_{max}/G = 0.06$. Using the shear modulus along the slip direction for partial dislocations we obtained $\sigma_{max}/G_{\langle 112 \rangle} \approx 0.08$ ($G_{\langle 112 \rangle} = 30.7$ GPa).

A new model for the nucleation and emission of a dislocation loop is presented here. The nucleation and emission process, which was presented in Figs. 1–3, is shown again in Fig. 4b. The required nucleation stress in the process of producing a shear dislocation loop has two components

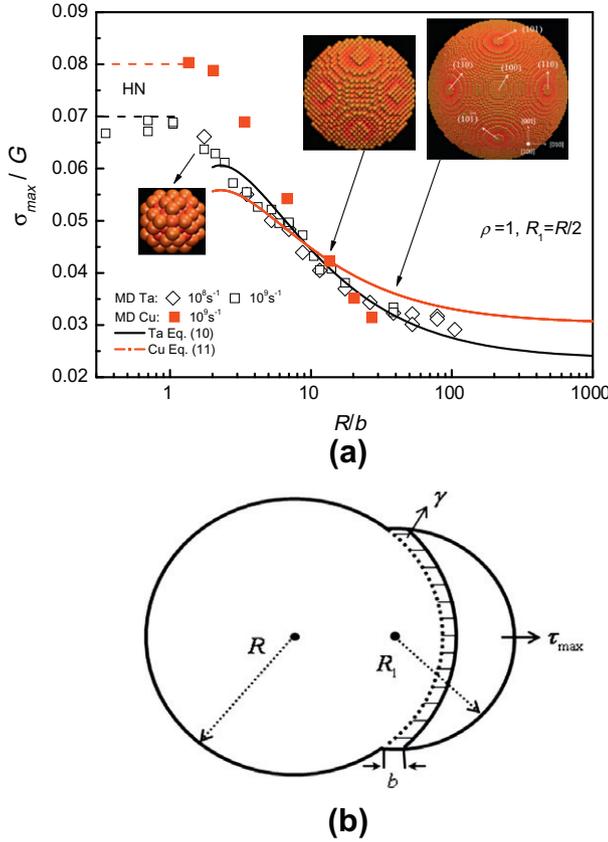a. The creation of a new surface step during the emission process.

Fig. 4. (a) Normalized maximum shear stress for defect generation as a function of normalized void radius R/b. The region marked HN corresponds to "homogeneous nucleation", with different shear moduli used for copper (fcc, $G_{\langle 112\rangle} = 30.7$ GPa) and tantalum (bcc, $G_{\langle 111\rangle} = 52.8$ GPa). (b) Schematic of dislocation emission from the void surface.

b. The stress required to generate and bow a dislocation loop to a radius R_1 that is a fraction of the void radius R.

The first component is evaluated using an approach akin to that of Rice and Thomson [2,36]: they assumed that the shear stress τ_1 involved in the creation of the surface step by emitting a dislocation over a distance ρb ($1 < \rho < 10$) has the form:

$$\tau_1 = \frac{2\gamma\rho b}{\pi[(\rho b)^2 + r^2]} \tag{1}$$

where γ is surface energy, and r is the distance between the dislocation and the void surface; at the moment of emission $r = 0$.

Thus one gets

$$\tau_1 = \frac{2\gamma}{\pi\rho b} \tag{2}$$

It is well known that the local stress concentration at the void surface is void-size independent, according to isotropic elasticity theory. Thus, a simple shear-stress threshold criterion for dislocation nucleation will be void-size

independent. On the other hand, MD simulation results show that the size of the generated shear dislocation loop R_1 is related to the void size R. Therefore, the shear stress $\tau 2$ required to generate and bow the dislocation to a semi-loop with a radius R_1, which has connection to void size R, is taken into consideration to account for the void-size dependence. A simple and general energy criterion is used to evaluate this shear stress, although there are more realistic Peierls-Nabarro based continuum models [37–39] available. The self energy of a full circular dislocation loop with radius R_1 has the form [40]:

$$U^{fullloop} = 2\pi R_1 A_0 \ln\frac{8R_1}{e^2\rho b} \tag{3}$$

For a full shear loop

$$A_0 = \frac{Gb^2(2-v)}{8\pi(1-v)} \tag{4}$$

where G is the shear modulus, and v is the Poisson ratio.

The energy of a semi-circular shear loop connected to a void can be assumed to have the form [40]:

$$U = \pi R_1 A_0 \ln\frac{8R_1}{e^2\rho b} + \pi R_1 A_0 \ln m \tag{5}$$

where m is a constant. The first term in Eq. (5) is the self-energy of a semi-circular shear loop and the second term accounts for the image interaction energy between the semi-circular loop and the void. The image interaction between a prismatic loop and a void has been calculated by Wolfer et al. [41] and Ahn et al. [42]. For a shear loop, which contains both edge and screw components, an explicit expression is still unavailable. Although image interactions between both an infinite straight edge [43] and screw dislocations [44] and a void have been derived in the form of infinite series (the distance from the dislocation line to the void center d must be larger than the void size R to avoid a singularity in the series), they are not applicable to the case of a shear loop attached to a void surface ($d < R$ for some sections of the shear loop). As an approximation of the image interaction between a semi-circular dislocation loop and a void, a value of $m = 2.2$ in Eq. (5) for the image interaction between a semi-circular shear loop and a crack tip ($\varphi = 0°$, $\psi = 0°$ in Fig. 17 in Anderson and Rice. [40]), which is the closest to the case studied here, is used.

The work done by the local shear stress τ_2 near the void surface has the form:
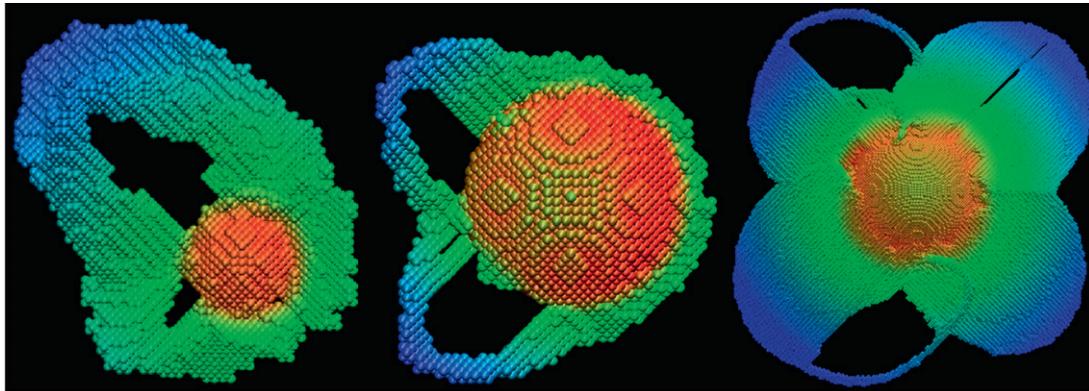
$$W = \tau_2\frac{\pi R_1^2}{2}b \tag{6}$$

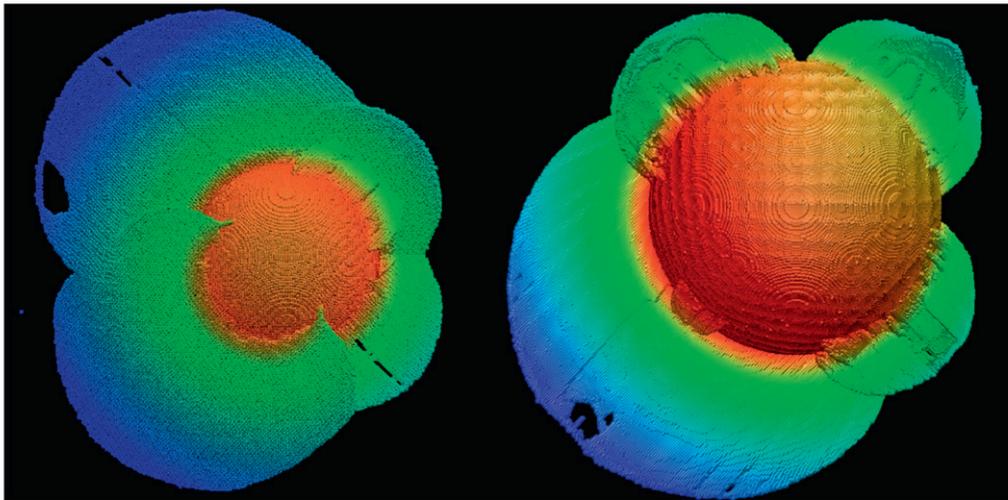and is equal to the energy of a semi-circular shear loop $W = U$. Equating Eq. (6) into Eq. (5) yields

$$\tau_2 = \frac{Gb(2-v)}{4\pi(1-v)R_1}\ln\frac{8mR_1}{e^2\rho b} \tag{7}$$

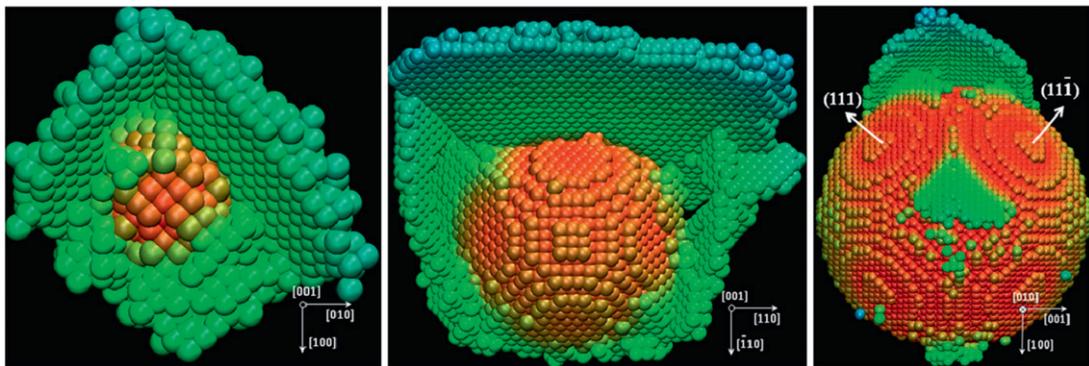Thus the total stress τ is equal to $\tau_1 + \tau_2$:

$$\tau = \frac{2\gamma}{\pi\rho b} + \frac{Gb(2-v)}{4\pi(1-v)R_1}\ln\frac{8mR_1}{e^2\rho b} \tag{8}$$

(a) Ta, $R = 1.5$ nm, $\varepsilon = 7.325\%$ (b) Ta, $R = 3.3$ nm, $\varepsilon = 4.75\%$ (c) Ta, $R = 7.5$ nm, $\varepsilon = 4.125\%$

(d) Ta, $R = 15$ nm, $\varepsilon = 3.695\%$ (e) Ta, $R = 30$ nm, $\varepsilon = 3.695\%$

(f) Cu, $R = 0.5$ nm, $\varepsilon = 10.9\%$ (g) Cu, $R = 2$ nm, $\varepsilon = 6.2\%$ (h) Cu, $R = 4$ nm, $\varepsilon = 4.5\%$

Fig. 5. Defects in tantalum (a–e) and copper (f–h) samples with different void radii R under uniaxial tensile strain. The loading direction [0 0 1] in (a–e) is perpendicular to the plane of the paper. The strain rate is 10^8 s^{-1} for Ta and 10^9 s^{-1} for Cu. The color scale indicates the radial distance from the void center. (For interpretation of the references to colour in this figure legend, the reader is referred to the web version of this article.)

For uniaxial strain loading the elastic stress field around a spherical void can be calculated and the maximum stress concentration occurs for the meridional stress at the equatorial plane, $1.7277\,\sigma_{zz}$ (using an isotropic Poisson ratio $\nu = 0.38$). Considering that the radial stress at the void surface is zero, the maximum local shear stress $\tau_{max} = (1.7277\,\sigma_{zz} - 0)/2 = 0.86\,\sigma_{zz}$, also at the equatorial plane. The maximum global shear stress σ_{max} is:

$$\sigma_{max} = (\sigma_{zz} - \sigma_{xx})/2 = 0.193\sigma_{zz} = 0.224\tau_{max} \qquad (9)$$

where $\sigma_{xx} = \nu/(1-\nu)\,\sigma_{zz}$ is the lateral normal stress. Thus

$$\frac{\sigma_{max}}{G_{\langle 111\rangle}} = \frac{0.224\tau_{max}}{G_{\langle 111\rangle}}$$

$$= 0.224\left[\frac{2\gamma}{G_{\langle 111\rangle}\pi\rho b} + \frac{b(2-\nu_{\langle 111\rangle})}{4\pi(1-\nu_{\langle 111\rangle})R_1}\ln\frac{8mR_1}{e^2\rho b}\right] \quad (10)$$

where the surface energy γ and Burgers vector b are 2.49 J m^{-2} [45] and 0.286 nm, respectively.

The same calculation can be applied to the fcc structure by adding a stacking fault energy term γ_{SF} to account for the stacking faults generated [15,16,24] during partial dislocation loop emission. The change in energy upon forming a stacking fault is equated to the work of dislocation. The energy is $\pi R_1^2\gamma_{SF}/2$. The work of advancing the partial dislocation, assuming that the mean advance is $\pi R_1/4$, is equal to $(2R_1 \times \pi R_1/4)b_p\tau_3$. Thus $\tau_3 = \gamma_{SF}/b_p$.

$$\frac{\sigma_{max}}{G_{\langle 112\rangle}} = \frac{0.165\tau_{max}}{G_{\langle 112\rangle}}$$

$$= 0.165\left[\frac{2\gamma}{G_{\langle 112\rangle}\pi\rho b_p} + \frac{b_p(2-\nu_{\langle 112\rangle})}{4\pi(1-\nu_{\langle 112\rangle})R_1}\ln\frac{8mR_1}{e^2\rho b_p} + \frac{\gamma_{SF}}{G_{\langle 112\rangle}b_p}\right]$$

$$(11)$$

For copper $G_{\langle 112\rangle} = 30.7$ GPa is the shear modulus of {1 1 1} planes shearing in the $\langle 1 1 2\rangle$ direction, $\nu_{\langle 112\rangle} = 0.182$, $b_p = 1/6\langle 1 1 2\rangle = 0.148$ nm is the Burgers vector of partial dislocation, $\gamma = 1.239$ J m^{-2} is the surface

energy, and $\gamma_{SF} = 44.4$ mJ m^{-2} [46] is the stacking fault energy. The stress concentration is 1.67 σ_{zz} ($\nu = 0.42$), and $\sigma_{max} = \sigma_{zz} - \nu/(1-\nu)\,\sigma_{zz} = 0.138\,\sigma_{zz} = 0.165\,\tau_{max}$.

The radius R_1 of the dislocation loop is taken, as a first approximation, to be half of the void radius R. Both results from Eqs. (10) and (11) are shown in Fig. 4a. Eq. (10) (for Ta) best matches the computational predictions in Fig. 4a for $\rho = 1$, which is consistent with the fact that bcc metals have smaller dislocation cores than fcc metals. This analytical model based on dislocation loop emission is not expected to be valid for void radii R/b smaller than 1–2, because the loop radius is smaller than the dislocation core and the analysis breaks down. Thus a cut-off was established at the maximum. MD simulation results under uniaxial strain loading along the [0 0 1] orientation for Cu [24] were recalculated at a strain rate of 10^9 s^{-1} and 300 K for comparison. The stress at the first dislocation emission, rather than the maximum stress, was taken. Eq. (11) (for Cu) shows a similar void dependence of the stress, but does not track the simulations as well as Eq. (10) for tantalum. One of the possible reasons is that for the [0 0 1] loading orientation, loop nucleation and early propagation are qualitatively and quantitatively different in fcc and bcc metals, as shown in Fig. 5f–h.

In view of the simplifying assumptions, the agreement between the computations and analytical model is considered satisfactory. Not included in the analytical model
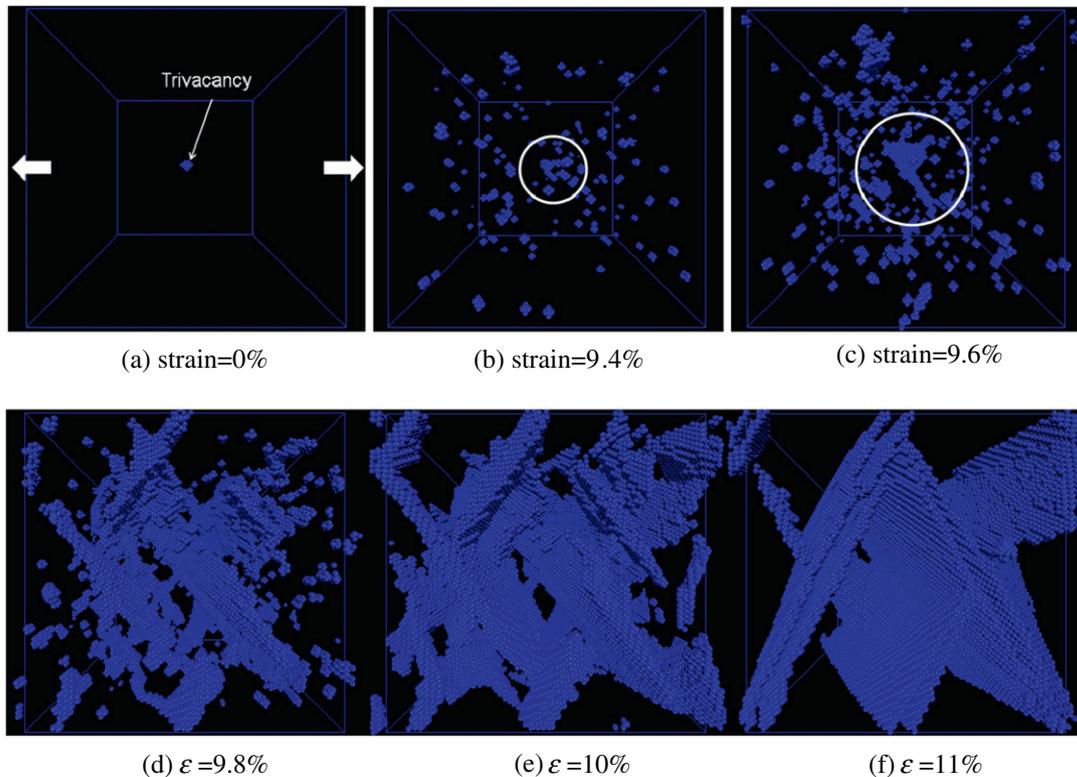

(a) strain=0%   (b) strain=9.4%   (c) strain=9.6%

(d) ε =9.8%   (e) ε =10%   (f) ε =11%

Fig. 6. Nucleation of plasticity at a tri-vacancy cluster surface in tantalum under uniaxial tensile strain along [0 0 1] (horizontal direction) at a strain rate of 10^9 s^{-1} (sample size $60 \times 60 \times 60$ a_0). Planar defects (stacking faults lying on {1 1 0} planes with a non-zero Schmid factor, namely (0 1 1), (0 $\bar{1}$ 1), (1 0 1) and ($\bar{1}$ 0 1)) nucleate at the tri-vacancy cluster (b and c), and then develop into (1 1 2) and ($\bar{1}$ 1 2) twins (e and f).

are the anisotropy, dislocation dynamics effects, and exact radius of the loop at the instant of emission.

Faceting of small voids may also play an important role in dislocation nucleation, as discussed for voids [24] and nano-indentation [47] in fcc metals. The effect of size on the geometry of voids in fcc structures were considered by Bringa et al. [24], who showed that the facets were {100} and {111}. This faceting is clearly seen in Fig. 5h, where the {111} planes are marked. The steps serve as initiation regions for the biplanar shear loop shown. The fourfold symmetry around the ⟨100⟩ axis was seen in the smaller voids. In comparison, voids in our single crystal Ta simulations are faceted with the {110} and {100} planes forming platforms at the extremities of the ⟨110⟩ axes. Three voids are shown in Fig. 4a and it can be seen that their shape approaches a spherical morphology as their size increases from 0.5 to 11 nm, since superimposed {110} planes more closely approach the ideal configuration. Hence, the following observations are applicable to both bcc tantalum and fcc copper:

1. The sphericity of a void decreases as the radius decreases. The void can be considered spherical for $R = 11$ nm. On the other hand, for $R = 0.5$ nm the void deviates significantly from sphericity and is a polyhedron.
2. The surface is composed of truncated steps which necessarily affect the generation of defects upon stressing. One such event is seen in Fig. 4a.

3.3. Defect generation and propagation

An earlier report on tantalum [23] showed that dislocation loops are emitted and propagate predominantly on {112} planes for a $R = 3.3$ nm void. Twinning also takes place along the {112} planes at a high strain rate 10^9 s^{-1}. Marian and Knap [48] observed loop generation (loading in [001]) at a 10.9 nm diameter void surface and twinning (loading in [$\bar{4}$ 8 1 9]) in Ta under uniaxial loading. Prismatic loops and a slip to twinning transition were
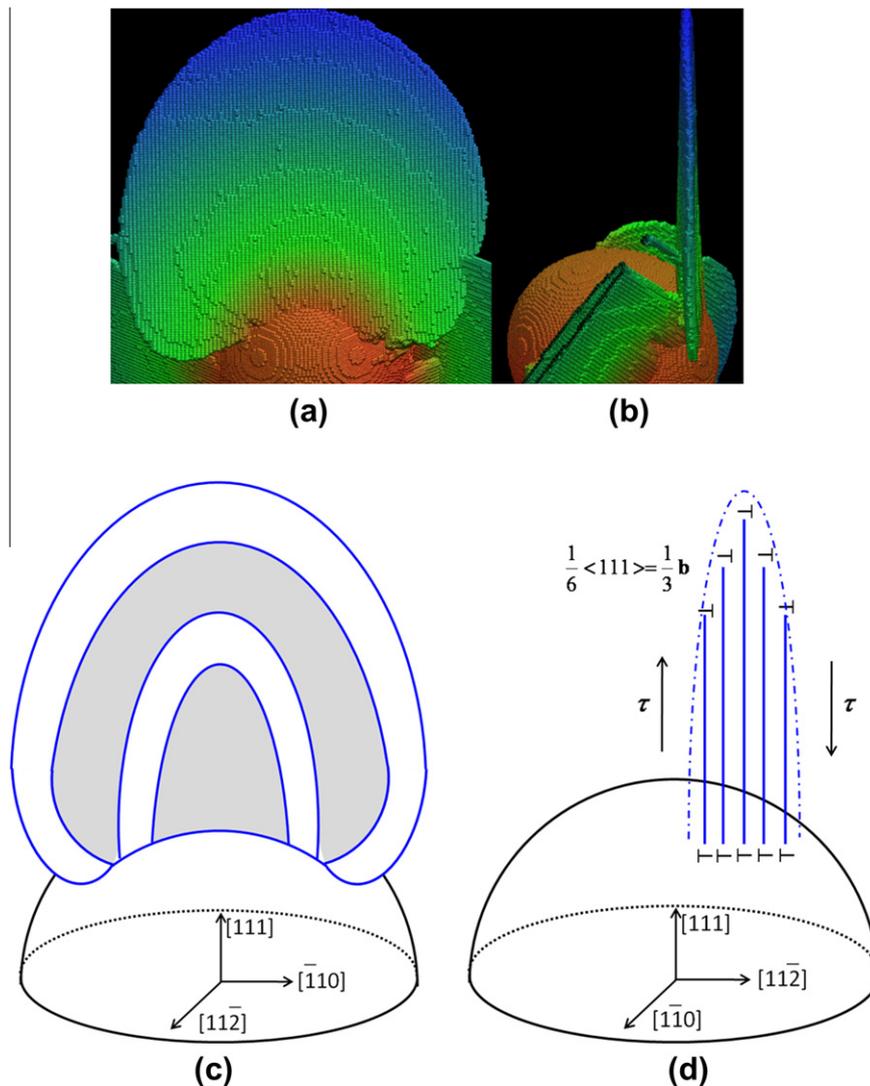

Fig. 7. (a) Front and (b) side views of twin boundaries in tantalum under uniaxial tensile strain at 10^8 s^{-1} ($R = 11$ nm). Note that the front of the expanding twin is thinner than the bottom. Schematic representation of (c) front and (d) side views of a twin with partial dislocations.

observed in Ta with void radii of 1.89 and 12.5 nm under hydrostatic tension by Rudd [34] when the strain rate was increased.

Fig. 5 shows the defects generated for different void sizes at a strain rate of $10^8 \, s^{-1}$. In Ta, with smaller voids, perfect dislocation loops are formed. For $R > 7.5$ nm twinning overcomes slip. This is seen in the sequence in Fig. 5a–e. This was also observed by Rudd [34]. Three void sizes for copper are shown in Fig. 5f–h for $R = 0.5$, 2, and 4 nm, respectively. The formation of biplanar loops [15,24] is clear in the three cases. Only the leading partial dislocations are formed.

3.3.1. Void sizes R/b < 1

Vacancy clusters are common in metals. The effect of pre-existing vacancies in shock loading has been studied before for fcc metals [49,50]. Recently Luo et al. [51] found a vacancy-induced decrease in the spall strength of fcc Cu. It is generally assumed that void initiation will occur at second phase particles, impurity clusters, nano-cracks, etc. However, in well-annealed, high purity metals initiation at small vacancy clusters might play a role in spall.

We reduced the void size to the size of a vacancy, di-vacancy and tri-vacancy (a $R = 0.3$ nm void has nine vacancies). Heterogeneous nucleation of stacking faults at the void surface (the required nucleation shear stress is still close to $0.07 G_{\langle 111 \rangle}$) was found to start for the tri-vacancy, developing into {112} twins, as shown in Fig. 6. Although the equilibrium concentration of mono-vacancies c_{eq} in Ta is only $\sim 10^{-46}$ at $T = 300$ K and is $\sim 5 \times 10^{-4}$ at the melting point $T = 3293$ K (the vacancy formation energy and entropy are 2.8 eV [52] and $2.2 k_B$ [53], respectively), and the equilibrium concentration of di-vacancies and tri-vacancies are much smaller due to the much higher energy of formation (5.56 and 8.16 eV [54]), it is still possible for their concentration to reach 10^{-5} at 300 K due to the generation of vacancies during plastic deformation [55]:

$$c_0 = 10^{-Y} \varepsilon + c_{eq} \qquad (12)$$

where ε is the plastic strain and Y is a parameter that can vary from 2 (for multiple slip) to 4 (for single slip). For a characteristic value of $\varepsilon \approx 0.1$ the concentration can be as high as 10^{-3}. These non-equilibrium vacancies can form complexes by migration, thereby decreasing their energy. Thus one can conclude that tri-vacancies are present in sufficient concentration after plastic deformation to nucleate voids. Similar results were obtained by Bringa et al. [24] for copper: tri-vacancies and di-vacancies acted as nucleation sites for voids, mono-vacancies did not.

3.3.2. Void sizes R/b > 1

In tantalum, for void sizes R/b from 1 to 7 ($R \approx 2$ nm), stacking faults developed into {112} twins after nucleation, as seen in Fig. 5a and b. For void sizes R/b from 7 to 17 ($R = 5$ nm), shear loops lying on {112} planes were formed (Fig. 5b). For larger void sizes a dominance of twinning was observed, as seen in Fig. 5c–e, although there

are also a number of {112} dislocation loops, including loops located at the rims of the formed twins (Fig. 5c) and secondarily emitted loops (upper right in Fig. 5e). The radius of curvature of the head of the dislocations (both perfect and twinning) increases with increasing void radius. It is also possible that emission of the second, third, and subsequent dislocations requires less stress if they are twinning dislocations. This could be one possible reason for the slip–twinning transition as R increases. Detailed views (front and side) of twins generated from the surface of a void ($R = 11$ nm) and a schematic of the twin are shown in Fig. 7. The twin thickness is approximately 12 atomic layers.

4. Summary and conclusions

1. A new mechanism for void growth in nanoscale voids is identified in both fcc and bcc metals. Dislocation loops are emitted from the void surface and expand as partial or perfect dislocations, evolve into a prismatic loops through reaction, or develop into twins.
2. The void size has a significant effect on the required stress to initiate plasticity in metals. The shear stress required to nucleate plasticity asymptotically approaches the theoretical shear strength $\sigma_{max}/G_{\langle 111 \rangle} = 0.07$ for tantalum (bcc) and $\sigma_{max}/G_{\langle 112 \rangle} = 0.08$ for copper (fcc). For $1 < R/b < 100$ the stresses decrease rapidly with increasing void size R/b and asymptotically approach a constant value (independent of void size) of $\sigma_{max}/G_{\langle 111 \rangle} \approx 0.0235$ for Ta.
3. An analytical model is proposed based on dislocation loop emission to account for this size effect. It tracks the simulations for tantalum closely and therefore provides a basis for extrapolation to larger voids (up to 300 nm) which are in the realm of second phase particles and inclusions.
4. Initiation of plastic flow takes place at voids as small as a tri-vacancy. These are present in sufficient concentration in metals by virtue of vacancy generation during plastic deformation.
5. In tantalum (a model bcc metal), void size has an effect on the defect generation sequence. For very small voids ($R/b < 7$) stacking faults are generated and then develop into {112} twins. For void sizes R/b from 7 to 17 ($R = 5$ nm) shear loops form at the void surface. For larger void sizes the dominant defects are {112} twins.

References

[1] Ritchie RO, Knott JF, Rice JR. J Mech Phys Solids 1973;21:395–410.
[2] Rice JR, Thomson R. Philos Mag 1974;29:73–96.
[3] Weertman J. Philos Mag 1981;43:1103–23.
[4] Christy S, Pak HR, Meyers MA. In: Murr LE, Staudhammer KP, Meyers MA, editors. Metallurgical applications of shock-wave and high-strain rate phenomena. New York: Marcel Dekker; 1986. p. 835.
[5] Kanel GI, Rasorenov SV, Fortov VE. In: Meyers MA, Murr LE, Staudhammer KP, editors. Shock-wave and high-strain rate phenomena in materials. New York: Marcel Dekker; 1992. p. 775.
[6] Meyers MA. In: Meyers MA, Armstrong RW, Kirchner HOK, editors. Mechanics and materials: fundamentals and linkages. New York: Wiley; 1999. p. 489–594.
[7] Edelson B, Baldwin W. Trans ASM 1962;55:230–50.
[8] Bringa EM, Caro A, Wang YM, Victoria M, McNaney JM, Remington BA, et al. Science 2005;309:1838–41.
[9] Van Swygenhoven H, Derlet PM, Hasnaoui A. Phys Rev B 2002;66:24101.
[10] Van Swygenhoven H, Derlet PM, Froseth AG. Acta Mater 2006;54:1975–83.
[11] Van Swygenhoven H, Caro A. Appl Phys Lett 1997;71:1652–4.
[12] Meyers MA, Mishra A, Benson DJ. Prog Mater Sci 2006;51:427–556.
[13] Kumar KS, Van Swygenhoven H, Suresh S. Acta Mater 2003;51:5743–74.
[14] Yamakov V, Wolf D, Phillpot SR, Mukherjee AK, Gleiter H. Nat Mater 2004;3:43–7.
[15] Traiviratana S, Bringa EM, Benson DJ, Meyers MA. Acta Mater 2008;56:3874–86.
[16] Meyers MA, Traiviratana S, Lubarda VA, Benson DJ, Bringa EM. J Mater 2009;61:35–41.
[17] Marian J, Knap J, Ortiz M. Phys Rev Lett 2004;93:165503.
[18] Marian J, Knap J, Ortiz M. Acta Mater 2005;53:2893–900.
[19] Seppälä ET, Belak J, Rudd RE. Phys Rev B 2005;71:064112.
[20] Bulatov VV, Wolfer W, Kumar M. Scripta Mater 2010;63:144–7.
[21] Lubarda VA, Schneider MS, Kalantar DH, Remington BA, Meyers MA. Acta Mater 2004;53:1397–408.
[22] Bringa EM, Lubarda VA, Meyers MA. Scripta Mater 2010;63:148–50.
[23] Tang Y, Bringa EM, Remington EM, Meyers MA. Acta Mater 2011;59:1354–72.
[24] Bringa EM, Traiviratana S, Meyers MA. Acta Mater 2010;58:4458–77.
[25] Plimpton SJ. J Comp Phys 1995;117:1–19.
[26] Dai XD, Kong Y, Li JH, Liu BX. J Phys Condens Matter 2006;18:4527–42.
[27] Tang Y, Bringa EM, Remington BA, Meyers MA. AIP Conf Proc 2012;1426:1255–8.
[28] Tsuzuki H, Branicio PS, Rino JP. Comput Phys Comm 2007;177:518–23.
[29] Kelchner CL, Plimpton SJ, Hamilton JC. Phys Rev B 1998;58:11085–8.
[30] Turley J, Sines G. J Phys D Appl Phys 1971;4:264–71.
[31] Moriarty JA, Belak JF, Rudd RE, Söderlind P, Streitz FH, Yang LH. J Phys Condens Matter 2002;14:2825–57.
[32] Finnis MW, Sinclair JE. Philos Mag A 1984;50:45–55.
[33] Ackland GJ, Thetford R. Philos Mag A 1987;56:15–30.
[34] Rudd RE. Philos Mag 2009;89:3133–61.
[35] Xu SZ, Hao ZM, Su YQ, Yu Y, Wan Q, Hu WJ. Comp Mater Sci 2011;50:2411–21.
[36] Weertman J. Dislocation based fracture mechanics. Singapore: World Scientific; 1996. p. 194–5.
[37] Rice J. J Mech Phys Solids 1992;40:239–71.
[38] Haviland GP, Ono K. J Appl Phys 1971;42:238–46.
[39] Schoeck G. Philos Mag A 1994;69:1085–95.
[40] Anderson PM, Rice J. J Mech Phys Solids 1987;35:743–69.
[41] Wolfer WG, Drugan WJ. Philos Mag A 1988;57:923–37.
[42] Ahn DC, Sofronis P, Kumar M, Belak J, Minich R. J Appl Phys 2007;101:063514.
[43] Ganeyev GZ, Turkebaev TE. Acta Metall 1988;36:453–7.
[44] Willis JR, Hayns MR, Bullough R. Proc R Soc Lond A 1972;329:121–36.
[45] Mishin Y, Lozovoi AY. Acta Mater 2006;54:5013–26.
[46] Mishin Y, Mehl MJ, Papaconstantopoulos DA, Voter AF, Kress JD. Phys Rev B 2001;63:224106.
[47] Ziegenhain G, Urbassek HM. Phys Rev B 2010;81:155456.
[48] Marian J, Knap J, Campbell GH. Acta Mater 2008;56:2389–99.
[49] Erhart P, Bringa EM, Kumar M, Albe K. Phys Rev B 2005;72:52104.
[50] Davila LP, Erhart P, Bringa EM, Meyers MA, Lubarda VA, Schneider MS, et al. Appl Phys Lett 2005;86:161902.
[51] Luo SN, Germann TC, Tonks DL. J Appl Phys 2010;107:56102.
[52] Li YH, Siegel DJ, Adams JB, Liu XY. Phys Rev B 2003;67:125101.
[53] Burton JJ. Phys Rev B 1972;5:2948–57.
[54] Zhang JM, Wen YN, Xu KW. Cent Eur J Phys 2006;4:481–93.
[55] Mott NF. Philos Mag 1952;43:1151–78.